Porous Silicon Nanodiscs for Targeted Drug Delivery

*Hashim Alhmoud, Bahman Delalat, Roey Elnathan, Anna Cifuentes-Rius, Arnaud Chaix, Mary-Louise Rogers, Jean-Olivier Durand, and Nicolas H. Voelcker**

There is a strong demand for techniques that allow the fabrication of biocompatible porous nanoparticles for drug delivery applications. In this work, a new method to fabricate size- and shape-controlled porous silicon (pSi) nanodiscs is described. The process relies on a combination of colloidal lithography and metal-assisted chemical etching. Height and diameter of the pSi nanodiscs can be easily adjusted. The nanodiscs are degradable in physiological milieu and are nontoxic to mammalian cells. In order to highlight the potential of the pSi nanodiscs in drug delivery, an in vitro investigation that involved loading of nanodiscs with the anticancer agent camptothecin and functionalization of the nanodisc periphery with an antibody that targets receptors on the surface of neuroblastoma cells is carried out. The thus-prepared nanocarriers are found to selectively attach to and kill cancer cells.

1. Introduction

Routes to fabrication of drug delivery nanovectors have been intensely investigated due to the obvious benefits of such nanocarriers over conventional drug administration methods.[1] Salient advantages include a reduction in the required drug dosage,[2–4] the availability of strategies that can increase the preferential accumulation of vectors within the targeted tissue due to the enhanced permeation and retention effect,[5,6] and the protection of the therapeutic agent from any degradation brought about by the physiological environment.[5–7] The literature contains many reports of delivery vectors from synthesized nanomaterials, taking advantage of the high surface-to-volume ratio that is fundamental to nanomaterials to load the therapeutic agent. These nanomaterials encompass liposomes,[8–10] polymeric nanoparticles,[1,11–13] micelles,[14,15] mesoporous silica,[6,16,17] and porous silicon (pSi) particles.[5,7,18,19]

Elemental silicon-based nanoparticles hold particular promise as drug-carrying nanovectors due to their biocompatibility and biodegradability, in contrast to the more commonly encountered mesoporous silica.[19,20] Furthermore, pSi nanoparticles offer very large surface-to-volume ratios for drug loading, and surface chemistry enabled control over degradation and hence drug release kinetics.[21] Finally, the fabrication conditions allow the adjustment of pore size and surface chemistry to the requirements of the drug to be loaded.[21]

pSi nanoparticle fabrication conventionally relies on anodization in hydrofluoric acid (HF) in order to produce the porous structure, followed by a postanodization step to fracture the porous layers into micro- and nanoparticles by means of extended ultrasonication or ball milling.[19,22,23] Following this conventional fabrication methodology, we have recently described the vectorization of a hydrophobic anticancer drug using antibody-functionalized pSi nanoparticles to cancer cells.[4]

Unfortunately, the conventional methods of pSi nanoparticle fabrication result in a considerable size distribution of particles even after time-consuming size-selection steps such as filtration or centrifugation. This size dispersion is disadvantageous for targeted delivery since studies[1,6,12,13,24,25] have shown that particle size and surface chemistry have a dramatic effect on nanoparticle behavior following administration. Hence, there is a need to develop approaches to prepare nanoparticles with narrow size distribution.

In addition to the effect of size, recent studies have suggested that the shape of nanoparticles also plays a major role in how those particles interact with cells in vitro.[26–30] Furthermore, particle shape also has a drastic effect on the preferential accumulation of the particles in certain organs when administered in vivo.[31,32] For example, discoidal nanocarriers are more prone to margination toward the blood vessel walls when circulating in the blood flow compared with spherical ones, since they are subjected to variable forces and torques causing a drift toward the walls and favoring their adhesion on the vascular endothelium. This margination process enhances the biodistribution of the nanoparticles, and thus increases their therapeutic efficacy.[7,29,33]

Several fabrication strategies have been recently developed that afford control of particle shape in addition to size. One highlight is the approach taken by the Ferrari group that affords discoidal pSi nanoparticles with controlled diameter that have been used successfully as nanocarriers.[7,34] Specifically, discoidal particles with size of 600 and 400 nm in diameter and thickness, respectively, showed a higher accumulation in tumor tissue and a longer circulation time than other sizes.[7] The

H. Alhmoud, Dr. B. Delalat, Dr. R. Elnathan, Dr. A. Cifuentes-Rius, Prof. N. H. Voelcker
Mawson Institute
University of South Australia
Mawson Lakes SA 5095, Australia
E-mail: nico.voelcker@unisa.edu.au
A. Chaix, Dr. J.-O. Durand
Institut Charles Gerhardt Montpellier (ICGM)
Université Montpellier 2
34095, Montpellier, France
Dr. M.-L. Rogers
Department of Human Physiology
Centre for Neuroscience
Flinders University
Bedford Park, SA 5042, Australia

DOI: 10.1002/adfm.201403414

downside of their method is arguably the reliance on expensive microfabrication processes such as photolithography, deep reactive ion etching, and chemical vapor deposition. Furthermore, a separate anodization step to define the pores is required.

Here, we present a fabrication strategy for pSi nanoparticles, which provides excellent control over the resulting size and shape of the particles. The strategy is based on a combination of cheap and easy to implement colloidal nanosphere lithography and Ag-catalyzed metal-assisted chemical etching (MACE) of silicon in a two-step fabrication process that inherently introduces porosity into the fabricated particles as Hochbaum et al.[35] and others[36–39] have previously demonstrated using highly doped silicon substrates (<0.005 Ω cm). Increasing the concentration of the oxidizing agent in the etching solution caused an increase in the average pore size, as well as a broadening of the pore size distribution.[38]

The resulting particles were discoidal and highly porous, and we thus chose to call them pSi nanodiscs (pSi NDs). Following the ND fabrication, an additional anodization step was employed to remove the NDs from the surface, while preserving the uniformity of the ND thickness.

2. Results and Discussion

2.1. Nanodisc Fabrication

The fabrication process is illustrated in **Scheme 1**. Colloidal nanosphere lithography was performed using convective assembly of polystyrene nanospheres (PSNS) on a highly doped flat Si substrate to create uniform, large scale, and dense hexagonal close-packed nanosphere monolayers (Scheme 1A).[40,41] This PSNS monolayer was etched in an O_2 plasma in order to reduce the diameter of the nanospheres and to create a nonclose-packed arrangement (Scheme 1B). This allowed the sputter deposition of an Ag layer in between the PSNS acting as a shadow mask (Scheme 1C). **Figure 1**A shows a scanning electron microscopy (SEM) image of the flat Si wafer with a self-assembled array of PSNS (1000 nm average diameter). The PSNS layer was etched with O_2 plasma to reduce the diameter of the nanospheres to ≈600 nm. An Ag layer of 40 nm thickness was then deposited on top. After PSNS removal, (Scheme 1D and Figure 1B), hexagonally arranged circular holes in the Ag layer remained. The next step was to perform MACE on the substrate using a mixture of HF and hydrogen peroxide (H_2O_2) (Scheme 1E) to produce an array of NDs attached to the Si wafer. The Ag layer was then easily removed by dipping the substrate in concentrated nitric acid for 1 min. The SEM image in Figure 1C confirm the formation of substrate-attached NDs of ≈600 nm diameter after MACE in HF/H_2O_2 for 30 min at room temperature, followed by the removal of the Ag layer using nitric acid. Figure 1D shows a close-up of one of these NDs and Figure 1E shows a cross section of a group of NDs attached to the Si substrate. It should be noted that the diameter of the resulting NDs corresponded to hole diameter in the Ag layer and the disc height was determined by the duration of the MACE process. By manipulating the diameter of the PSNS prior to Ag deposition, it was possible to precisely control the diameter of the resulting NDs, reaching diameters of 150 nm at the lower end as shown in Figure S1D–F, Supporting Information. The pSi particles depicted in Figure S1D (Supporting Information) of 150 nm diameter have a deformed discoidal shape due to the fact that sputtered Ag granules often nucleate with sizes ranging from 80 to 100 nm,[42] therefore it is hard to define patterns at such sizes. Logeeswaran et al.[42], on the other hand describe a method by which Ag granule sizes can

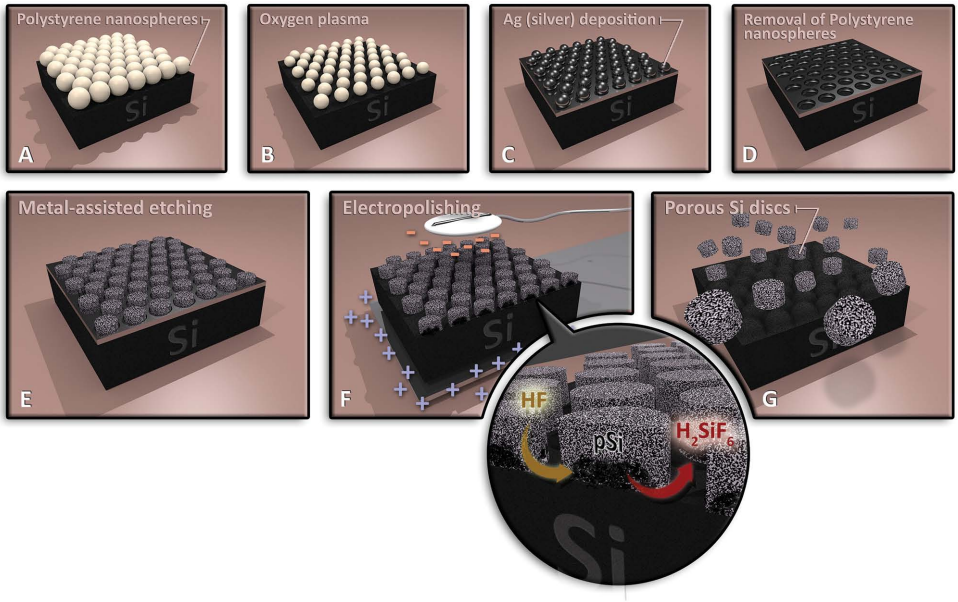

Scheme 1. Schematic of the multistep fabrication process. A) The self-assembly of PSNS onto a Si wafer. B) Size reduction of PSNS by O_2 plasma treatment. C) Ag deposition and D) removal of the PSNS layer. E) Schematic of the array of pSi NDs on the Si wafer after MACE in HF/H_2O_2. F) The removal of the Ag layer and the subsequent electropolishing step done to lift off the pSi NDs from the Si wafer using electropolishing. G) The pSi NDs after removal from the Si wafer.

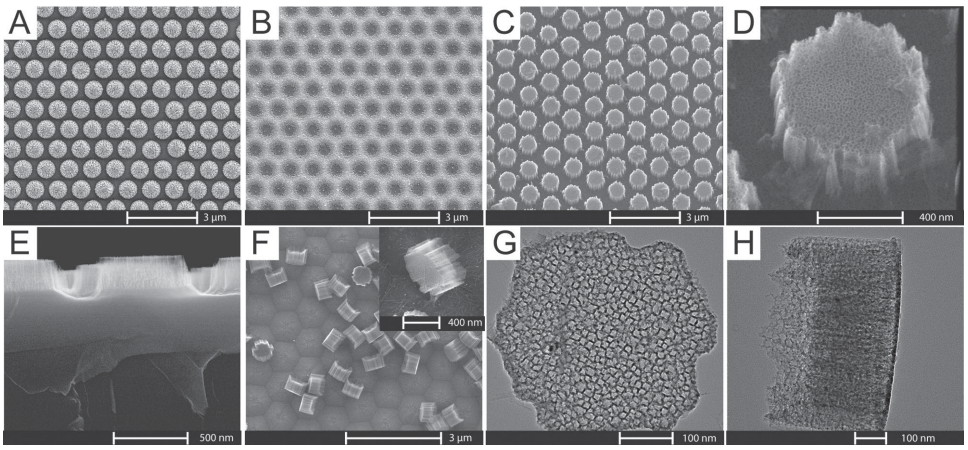

Figure 1. SEM and TEM images acquired after the different fabrication steps. A) Array of 1000 nm PSNS on flat Si after O_2 plasma treatment and Ag deposition. B) Ag layer after removal of PSNS showing the presence of holes in the metal layer. C) pSi ND array after MACE in HF/H_2O_2 and removal of Ag layer. Scale bar for (A–C) is 3 μm. D) A close-up image of one of the pSi NDs (scale bar = 400 nm). E) Cross section of pSi NDs (scale bar = 500 nm). F) pSi NDs randomly spread across the Si surface following electropolishing (scale bar = 3 μm). The inset shows a closeup of one of the pSi NDs lying on its side (scale bar = 400 nm). G) TEM top view of an individual pSi ND (scale bar = 200 nm). H) TEM side view of an individual pSi ND (scale bar = 100 nm).

be reduced to 15–20 nm but this was not investigated in this work. It was straightforward to define patterns ranging in size between 280 and 750 nm as is depicted in Figure S1E,F (Supporting Information). Furthermore, by changing the duration of the etching reaction, we were able to finely tune the etching depth and therefore ND height. Figure S1A–C (Supporting Information) shows SEM images of A) 150 nm thick NDs, B) ≈1 μm long semirods, and C) 1.3 μm rod-shaped particles produced by MACE for 15, 60, and 120 min, respectively. The results for different etching parameters are summarized in Table S1 (Supporting Information). The control over the size and shape of the produced ND by this approach is especially interesting given the fact that each tumor might need a personalized nanoparticle design depending on its features. It is known that tumors are both hemodynamically and pathologically different to one another, which requires the engineering of a drug delivery nanovector to reach the tumor of interest in the adequate conditions.[29,33]

In order to remove the NDs from the surface in a controlled manner, an electropolishing step in 1:1 HF/ethanol was employed to disrupt the interface between the porous structure of the NDs and the solid bulk Si substrate (Scheme 1F). The final step of the process therefore aimed at generating a suspension of intact NDs with uniform diameter and height (Scheme 1G). Indeed, following the electropolishing step, the pSi NDs detached from the surface and are shown in Figure 1F lying on the electropolished Si wafer in random orientations but with uniform size and height. The inset shows an SEM closeup of one of the detached pSi NDs lying on its side. Figure 1G,H depict transmission electron microscopy (TEM) images of a single ND from the top and side, respectively. From the TEM images, an average pore size of 15 ± 5 nm was obtained. And a surface area of 185 m^2 g^{-1} was determined from a N_2 adsorption/desorption isotherm fitted to a Brunauer–Emmett–Teller model. SEM and TEM images confirmed the production of NDs with a diameter of ≈600 and 400 nm in thickness, with narrow size distribution of just ±5% in both parameters. These values confirm the control over the size and shape achieved by this approach and the large degree of homogeneity that was obtained in comparison with the conventional method to produce pSi nanoparticles where particle size distributions of ± 50%–100% are commonly reported.[23,43,44]

Furthermore, several NDs were prepared with increasing concentrations of H_2O_2 in order to investigate the effects on ND pore size and morphology (**Figure 2**). NDs etched in a solution containing 4.8 M HF/0.1 M H_2O_2 showed an increase in structural roughness when compared with NDs etched in 0.01 M H_2O_2 (Figure 2A). TEM analysis showed a noticable increase in the average pore size (27 ± 7 nm compared with 15 ± 5 nm for 0.01 M H_2O_2). When NDs were etched in 0.2 M H_2O_2, an even more pronounced roughening of the structures was observed and the pore size increased to 47 ± 16 nm. A noticeable increase in the pore size distribution was also observed and was attributed to pore collapse. Figure 2C shows a cross-section SEM scan of an array of NDs that were etched first in a solution of 4.8 M

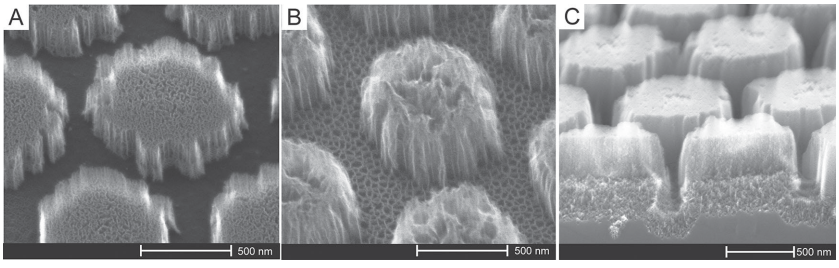

Figure 2. SEM images acquired after fabrication of pSi NDs using two different etching solutions. A) NDs etched using a solution of 4.8 M HF and 0.1 M H_2O_2, B) NDs etched using a solution of 4.8 M HF and 0.2 M H_2O_2, and C) a cross-sectional view of NDs etched first in a solution 4.8 M HF/0.01 M H_2O_2, followed by etching in 4.8 M HF/0.2 M H_2O_2 where the interface between the layers with two different porosities is visible (scale bar = 500 nm).

HF and 0.01 M H_2O_2 for 30 min, followed by 2 min etching in 4.8 M HF and 0.2 M H_2O_2. The change in H_2O_2 concentration drastically impacted on the porosity of the structures, where the interface between the top porous layer and the bottom ultraporous layer was highly visible. This illustrates nicely the flexibility that MACE offered in terms of controlling porosity and pore size.

2.2. ND Functionalization and Drug Loading

In order to exemplify the potential of the size- and shape-controlled pSi nanoparticles, their ability to selectively target cancer cells and deliver a cytotoxic drug was tested.

A surface functionalization approach was required to a) slow down ND degradation and b) enable the attachment of cell targeting antibodies. Here, two antibody conjugation routes were employed, namely using carboxylic acid activated by N-hydroxysuccinimide (NHS) resulting in nonoriented antibody conjugation via amine groups, and employing semicarbazide chemistry with periodate-oxidized antibodies, which results in oriented attachment via the antibody's Fc region.[5,45] In order to functionalize the NDs, hydrosilylation reactions with undecylenic acid (UA) and *tert*-butyl-2 [(allylamino)carbonyl]hydrazine-carboxylate (SC), respectively, were carried out on freshly prepared silicon hydride-terminated particles. A schematic of the two chemical modification routes is shown in Scheme S1, Supporting Information. Infrared (IR) characterization confirmed the successful functionalization of the pSi NDs (Figure S2, Supporting Information). The IR spectrum for untreated NDs showed a small peak at 2245 cm^{-1} corresponding to Si—H stretching vibrations as well as a silicon oxide peak at 1100 cm^{-1}, indicating that the NDs were partially oxidized when exposed to atmospheric oxygen during the sample preparation for IR spectroscopy. Tert-butyloxycarbonyl (BOC)-protected semicarbazide-functionalized NDs (ND-SC) exhibited peaks at 1655 and 1700 cm^{-1} corresponding to C═O stretches from the urea and carbamate groups, respectively. Additional peaks were observed at 2850 and 2920 cm^{-1} and attributed to C—H stretching vibrations from the aliphatic chains. In contrast, UA-functionalized NDs (ND-UA) showed peaks at 1720 cm^{-1} (C═O stretching vibration from the carboxylic acid) and peaks at 2850 and 2920 cm^{-1} assigned to C—H stretching vibrations.

In terms of degradation rates, surface functionalization provided protection for the NDs and reduced the rate of degradation relative to the nonfunctionalized NDs. Nonfunctionalized NDs showed a rate of degradation of 2.3 mM h^{-1} that was equivalent to 54% of the total amount of silicic acid produced as a result of complete degradation. These NDs degraded fully after 2 h, which was confirmed through visual observation, where the solution color changed from a murky brown to colorless.The rate of degradation was dramatically decreased to < 1% for both ND-SC (18×10^{-3} mM h^{-1}) and ND-UA (27×10^{-3} mM h^{-1}) (**Figure 3**). These results demonstrate that the surface functionalization removed most of the Si—H groups that are responsible for pSi degradation by oxidative hydrolysis.[46]

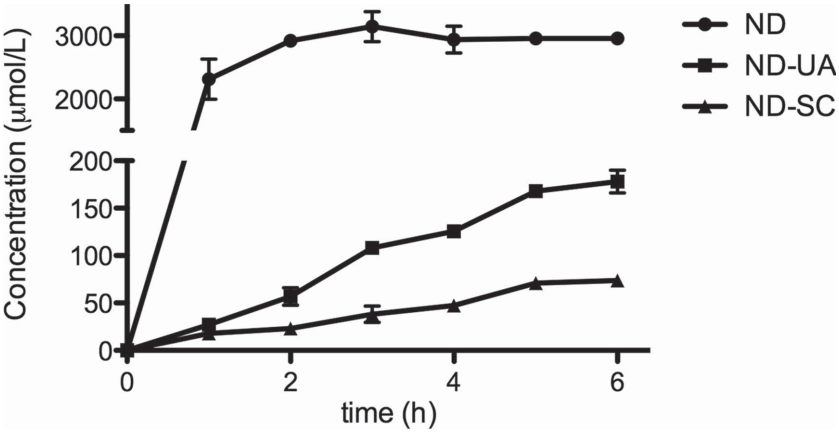

Figure 3. Degradation of pSi NDs as determined by silicic acid release over 6 h in Tris buffer (pH = 7.2) at room temperature. A) Silicic acid release for nonfunctionalized pSi NDs. B) Silicic acid release for pSi NDs functionalized with semicarbazide and undecylenic acid chemistries. $n = 3$.

We then examined the loading of the anticancer drug camptothecin (CPT) into the pores of the pSi NDs. CPT is a hydrophobic alkaloid compound targeting DNA topoisomerase I, an important enzyme involved in the removal of DNA supercoiling during DNA transcription.[47,48] Topoisomerase inhibitors are popular targets for cancer chemotherapy. CPT entered phase I and II clinical trials but had to be abandoned due to severe toxic side effects.[49] CPT is therefore an excellent candidate for vectorization with nanoparticles, in order to avoid such drawbacks.[50]

Prior to CPT loading, ND-SC was deprotected via removal of the BOC-group to form ND-SC-deprotected or ND-SC-DP for short. Similarly, ND-UA was NHS activated to form ND-UA-NHS. High-performance liquid chromatography (HPLC) was used to determine the amount of CPT loaded into the pSi NDs. The ND-UA-NHS gave a total loading of 2.09 mg mg^{-1} compared with the 1.88 mg mg^{-1} loaded shown by the ND-SC-DP (Table S2, Supporting Information). These are very high loading rates as compared with previous works including Secret et al.[5] where the authors obtained loadings of ≈0.1 mg mg^{-1}. Additionally, a work by Lu et al.[51] reported a maximum CPT loading value of around 600 ng mg^{-1} in porous silica nanoparticles. On the other hand, Kinnari et al.[52] reported on the loading of thermally oxidized and thermally carbonized pSi particles with the hydrophobic drug itraconazole showing loadings of around 112 and 113 μg mg^{-1} for the thermally carbonized and thermally oxidized particles, respectively.

Figure 4 displays the release kinetics of CPT from the pSi NDs over 24 h in cell culture medium at 37 °C, reported as the percentage of the total CPT loaded. The release kinetics for all NDs showed a burst release that occurs immediately after adding the NDs to the cell culture media. Such behavior is not surprising, since it is known that nanoparticles interact with biological fluids forming a protein corona, which can promote payload release.[53] At the same time, drug molecules adsorbed onto the surface and held by weak intermolecular forces can contribute significantly to the burst release percentage

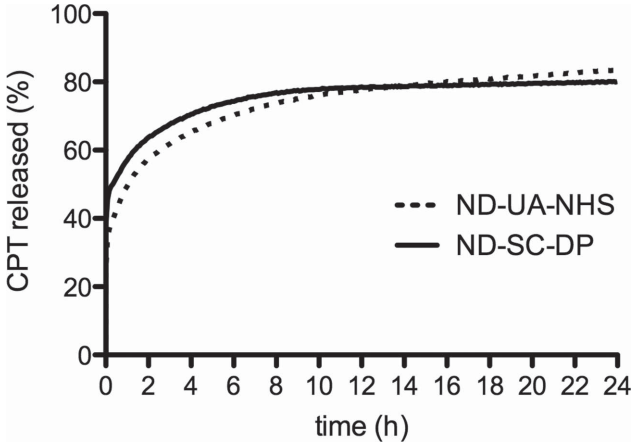

Figure 4. CPT release from pSi NDs with different surface chemistry. Drug release in cell culture media at 37 °C was followed over the first 24 h. The amount released is depicted as a percentage of the total amount loaded for each set of NDs. The two sets of functionalized NDs include NHS-activated undecylenic acid-functionalized NDs (ND-UA-NHS) and deprotected-semicarbazide-functionalized NDs (ND-SC-DP).

regardless of the type of media that the release is occurring in.[54] The burst release was around 50%–55% after ≈2 h, followed by sustained release over the rest of the measurement period. The CPT burst release for ND-UA-NHS was less extensive than for ND-SC-DP. After the 4 h time point, the total amount of CPT released from both ND sets started to equalize, culminating in a slightly larger percentage of CPT released by ND-UA-NHS (83%) relative to ND-SC-DP (80%) by the end of the measurement period (24 h). Therefore, our pSi NDs showed extended release profiles compared with the pSi nanoparticles by Secret et al.[5] where 80% of CPT was released after only 3 h. In comparison, Lu et al.[51] reported on a maximum of 10% release of CPT from porous silica nanoparticles within 6 h. However, those release experiments were performed in PBS instead of cell culture medium.

2.3. Antibody Immobilization and Cell Targeting

For the ND-SC-DP, the antibody had to be periodate oxidized in order to generate an aldehyde group on the carbohydrate side chain on the antibody's Fc fragment. Covalent binding of an antibody on the functionalized ND-SC-DP and ND-UA-NHS was confirmed by employing a Dylight 549-labeled mouse anti-human IgG antibody (Figure S3, Supporting Information). The results showed that the labeled antibody failed to attach to non-functionalized NDs, whereas it was clearly bound to the functionalized NDs.

Cancer cell targeting was explored using MLR2 anti-p75 antibodies targeting the p75NTR neurotrophin receptor that is expressed on the surface of neuroblastoma cells (SH-SY5Y).[55–57]

We investigated both semicarbazide and NHS chemistries to attach the MLR2 antibody. The antibody was labeled with fluorescein isothiocyanate (FITC) to evaluate selective attachment of MLR2 antibody-functionalized NDs to SH-SY5Y cells. The BSR cell line, a clone of baby hamster kidney cells, which are not able to express p75NTR, were used as a negative control. Note that for these experiments, the NDs were not loaded with CPT. After 30 min of incubation with the NDs, the cells were rinsed and the culture medium replaced. Furthermore, the SH-SY5Y and BSR cells were stained and characterized using confocal fluorescence microscopy (**Figure 5**). It was apparent from Figure 5A,C that the MLR2 antibody-functionalized NDs failed to attach to the control BSR cells since there was no green fluorescence present. In contrast, green fluorescing spots were scattered around the cell nuclei of SH-SY5Y cells (Figure 5B,D), especially for the ND-SC-DP. In fact, a total number of 50 ± 8 NDs with MLR2 antibody attached through the semicarbazide functionality per cell were counted, whereas only 30 ± 3 NDs/cell were observed for the ND-UA-NHS. Therefore, a higher efficiency in reaching the target cell was obtained when the MLR2 was immobilized on the NDs via semicarbazide chemistry. The selective attachment of the MLR2 antibody-functionalized NDs was also confirmed in SEM images (Figure 5E–F).

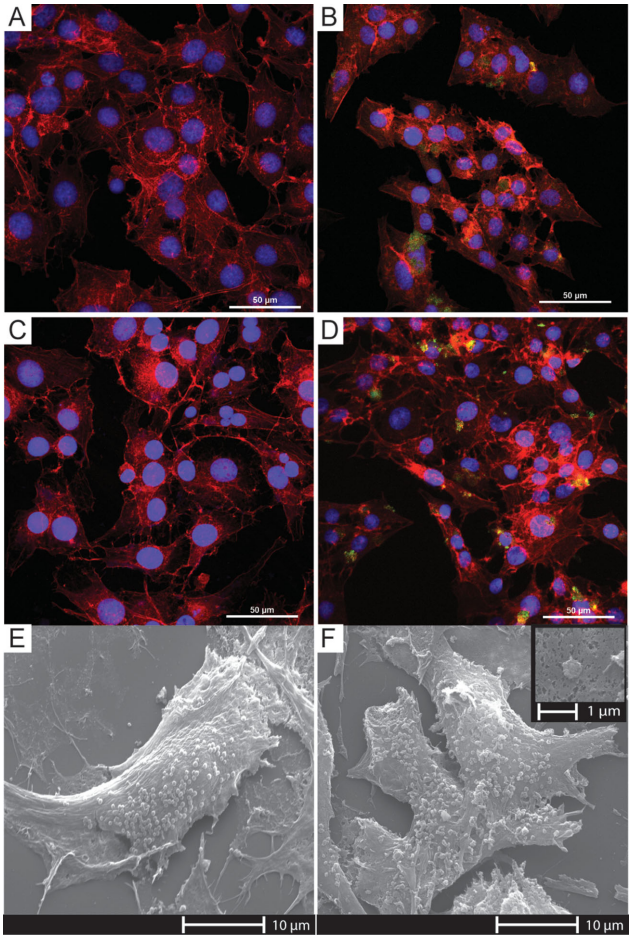

Figure 5. Interaction of MLR2 antibody-functionalized pSi NDs with cells. A–D) Optical confocal fluorescence microscopy images (blue = nucleus, red = cytoplasm, green = NDs, scale bar = 50 µm). A,B) BSR cells and SH-SY5Y cells, respectively, after treatment with ND-UA-MLR2. C,D) BSR cells and SH-SY5Y cells, respectively, after treatment with ND-SC-MLR2. Last two images are SEM images SH-SY5Y cells after treatment with E) ND-UA-MLR2 and F) ND-SC-MLR2 (scale bar = 10 µm). Inset: Zoom in of the ND-SC-MLR2 attached on the cell.

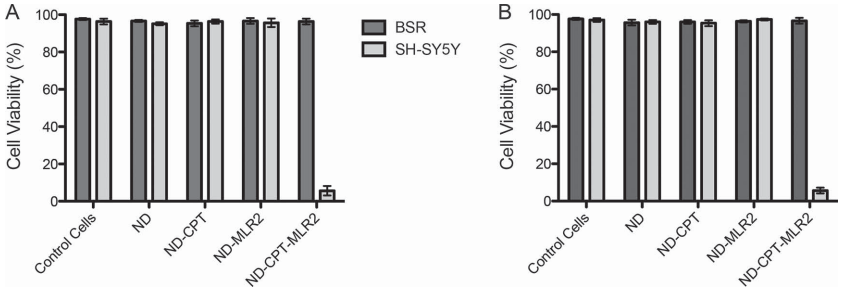

Figure 6. Viability of SH-SY5Y neuroblastoma cells targeted by antibody- and drug-loaded NDs. SH-SY5Y cells (contain p75NTR) and BSR (lack p75NTR) cells were incubated with 50 μg mL^{-1} pSi NDs. After 30 min, the cell culture medium was replaced to remove unattached NDs. For each sample, viability analysis was performed in triplicates. Panel A) relates to pSi NDs with NHS functionality, whereas B) shows results of pSi NDs with semicarbazide chemistry. Control cells were cells grown in media without any treatment. Cells were treated with pSi NDs (ND), CPT-loaded pSi NDs (ND-CPT), MLR2 antibody-functionalized pSi NDs (ND-MLR2), and pSi NDs loaded with CPT and functionalized with MLR2 antibody (ND-CPT-MLR2).

2.4. Targeted Drug Delivery to Neuroblastoma Cells

Finally, we evaluated the effect of CPT loaded and MLR2 antibody-functionalized pSi NDs on SH-SY5Y and BSR cells. Both cell lines were treated with nonfunctionalized NDs (ND), CPT-loaded pSi NDs (ND-CPT), pSi NDs functionalized with MLR2 antibody (ND-MLR2), and pSi NDs loaded with CPT and functionalized with MLR2 antibody (ND-CPT-MLR2). The experiment was carried out for both functionalization chemistries used, semicarbazide (ND-SC-DP) and NHS (ND-UA-NHS). Note that for these experiments, CPT loading was carried out first, followed by antibody immobilization. Cells were incubated with 50 μg mL^{-1} of pSi NDs for 30 min, followed by replacement of the culture medium to remove any unbound NDs.[4] The cells were then incubated for 2 d, after which a lactose dehydrogenase (LDH) assay was performed to determine the cytotoxicity for each treatment (**Figure 6**).

The results showed that nonfunctionalized NDs were nontoxic to both BSR and SH-SY5Y cells. The same was true for the ND-MLR2. Interestingly, ND-CPT were also nontoxic to both cell types, and we attribute this result to the fact that the ND dispersion was removed from the cell culture after 30 min of incubation and replaced with cell culture medium not containing NDs. However, strong toxicity was observed in the neuroblastoma cells when incubated with CPT-loaded NDs that also displayed the MLR2 antibody. Interestingly, pSi NDs functionalized with the semicarbazide and UA showed the same toxicity effects (5.6% remaining cell viability in both cases) despite the different antibody attachment chemistry, suggesting that with both functionalities the dose of CPT released on the target cells reached the same stage of lethality. This is despite the observation that ND-SC-DP more avidly attached to target cells. Perhaps the slightly higher CPT loading in ND-UA-NHS was able to offset the lower avidity in attachment to cells.

Finally, the selectivity of the antibody targeting was also effectively demonstrated in this experiment since BSR cells lacking the p75NTR receptor remained highly viable after incubation with CPT loaded and antibody-functionalized NDs (cell viability > 96%).

3. Conclusions

In conclusion, we have demonstrated a novel fabrication method for size- and shape-controlled pSi nanoparticles utilizing simple colloid nanosphere lithography, coupled with MACE. The method resulted in nanoparticles with discoidal shape, hence termed NDs and could be produced with a diameter of 150–750 nm and heights varying from 150 nm to over 1 m. The pSi NDs were highly porous, degradable and could be loaded with a large payload of the anticancer drug CPT (up to 2 mg mg^{-1}). Two types of bioconjugation routes were explored to compare nonoriented and oriented antibody immobilization on the pSi NDs. The ability of MLR2 antibody displaying pSi NDs loaded with CPT for targeted drug delivery was confirmed by the selective attachment to and killing of SH-SY5Y neuroblastoma cells. Overall, our study opens new vistas for the field of cancer nanovectors.

4. Experimental Section

Materials and Reagents: Silicon wafers (3in. diameter, boron-doped p++ ≤ 0.001 Ω cm) were purchased from Siegert (Germany). Sulfuric acid (H_2SO_4, 95%–97%) and HF (48%) were purchased from Scharlau Chemie (Chem-Supply Pty. Ltd. Australian representation). H_2O_2 (30%) was purchased from Merck (Australia). The PSNS solution was purchased from Polysciences (USA) and concentrated 10× by centrifugation. All other chemicals were purchased from Sigma-Aldrich (Australia) unless otherwise stated.

Fabrication of NDs: Fresh flat silicon wafers were first cleaned in a solution of Piranha (2:1 H_2SO_4:H_2O_2, 85 °C) for 1 h, followed by rinsing in MilliQ water and drying with a N_2 gas jet. 1 mL of PSNS solution (1.0 μm) was concentrated by centrifugation at 12 000 rpm, and 900 μL of the supernatant was collected and removed. The remaining solution was vortex mixed. A convective assembly setup was used to generate a PSNS monolayer by coating 60 μL of concentrated PSNS solution (per wafer) at a speed of 150 μm s^{-1}. The coated wafer was then subjected to O_2 plasma etching using a HHV TF600 sputter coater fitted with a PLC control system. The O_2 plasma (50 W RF, 15 sccm O_2, 2.00×10^{-2} mbar) was used to treat the wafer for 25 min to reduce the PSNS array diameter. The same system was then used to sputter coat a thin layer of Ag (40 nm, 100 W DC, 10 sccm Ar, 1.00×10^{-2} mbar). Finally, the PSNS layer was removed by ultrasonication in MilliQ water for 1 min and the wafers were etched in a solution of HF (4.8 M) and H_2O_2 (0.01 M) in MilliQ water (100 mL) for 30 min at room temperature. The Ag layer was removed by dipping the wafer in concentrated HNO_3 for 1 min.

ND Liftoff and Processing: Using a standard pSi etching cell, the pSi NDs were lifted off via electropolishing in a solution of 1:1 HF:ethanol using a current of 360 mA cm^{-2} for up to 20 s, followed by ultrasonication for 10 s. The NDs were then harvested by centrifugation at 18 000 rpm using a Sigma 3–18 K centrifuge (John Morris Scientific, Australia), resuspended in ethanol and washed with ethanol several times to remove any remaining HF solution. For surface area characterization, 10 mg of sample was analyzed using N_2 adsorption/desorption volumetry at –196 °C using a Quadrasorb Surface Area Analyzer (Quantachrome, USA). The sample was degassed overnight at 300 °C prior to analysis.

4.1. pSi NDs Functionalization with Semicarbazide

a) *Hydrosilylation and Deprotection*: A solution of *tert*-butyl-2 [(allylamino) carbonyl]hydrazine-carboxylate was prepared in dry tetrahydrofuran (THF) at a concentration of 0.1 M, followed by several cycles of freeze–pump–thaw to remove any trapped O_2. The pSi NDs (100 µg) were washed twice with THF and injected into the semicarbazide solution under an N_2 atmosphere and allowed to react at 85 °C under reflux for 4 h to form ND-SC. This was followed by rinsing the ND-SCs twice with THF, once with ethanol, and once with dichloromethane (DCM, CH_2Cl_2). The ND-SC were then collected through centrifugation and dispersed in a 2 mL mixture of DCM:TFA (trifluoroacetic acid) at 3:2 v/v in order to remove the BOC protecting group (Figure S2, Supporting Information). The solution was left in the dark for 4 h under agitation to complete the reaction. The pSi ND-SC-DP in solution were then washed with DCM twice, with ethanol once, and then dried.

b) *Oxidation of Antibody*: MLR2 antibody solution (2 mg mL^{-1}) was kindly provided by Marie-Louise Rogers (Flinders University, Australia) in phosphate buffer saline (pH 7.4).[57,58] An oxidizing solution was prepared by dissolving sodium periodate in a buffer solution composed of 20 mM sodium acetate (NaAcO) and 0.15 M sodium chloride (NaCl) at pH 5.0 at a concentration of 20 mM. Both the antibody and the periodate solutions were mixed together at a 1:1 ratio and allowed to react in the dark at room temperature for 30 min under agitation. The oxidation reaction was then quenched by addition of ethylene glycol at 1:4 v/v of the antibody solution. Excess oxidant was removed by dialysis using SnakeSkin™ tubing with Mw = 10 000 Da. The solution was dialyzed against 2 L of the NaAcO/NaCl buffer for 2 h followed by three successive steps of dialysis against a buffer solution composed of 0.1 M monopotassium phosphate (KH_2PO_4, pH 6.5), using 2 L of buffer for 2 h at each step.

c) *Drug Loading and Antibody Attachment*: The ND-SC-DP were immersed in a solution of CPT dissolved in dry dimethylformamide (DMF) at a concentration of 2.5 mg mL^{-1}. The pSi NDs were incubated in the solution in the dark for 24 h, followed by centrifugation and the removal of DMF through evaporation under vacuum. The ND-SC-DP were then rinsed with ethanol and dried under vacuum (ethanol used for rinsing was kept for CPT concentration measurement). The oxidized antibody solution was adjusted to pH 6.0 using HCl and 100 µg of pSi NDs were added to the solution and allowed to react for 30 min in the dark at room temperature while agitating. The pSi NDs were then finally centrifuged and resuspended in 1 X PBS (pH 7.4).

4.2. ND Functionalization with Undecylenic Acid

a) *Hydrosilylation*: UA was liquefied at 60 °C under an N_2 atmosphere, while allowing the N_2 jet to bubble through the liquid for 5 min. Freshly made pSi NDs (100 µg) were washed with ethanol and allowed to dry until less than 100 uL of ethanol remained with the NDs suspended in it. The remaining ethanol containing the NDs was injected directly into 2 mL of liquid UA and allowed to react for 4 h at a temperature of 120 °C. The pSi NDs were then extracted via centrifugation at 18 000 rpm and washed with ethanol three times.

b) *EDC/NHS Activation*: The UA-functionalized NDs (ND-UA) were extracted from ethanol using centrifugation at 18 000 rpm and rinsed with 1X PBS (pH 7.4) twice, followed by removal of the PBS. A solution of 10 mM NHS was prepared in 1X PBS. At the same time, a 10 mM solution of ethyl(dimethylaminopropyl) carbodiimide in 1X PBS was prepared. The two solutions were mixed at a 1:1 ratio to form 2 mL of solution which was then added to the ND-UA. The NDs were resuspended in solution and the mixture was allowed to react for 1 h to form ND-UA-NHS, following which the pSi NDs were recovered by centrifugation and washed with MilliQ water once.

c) *Drug Loading and Antibody Attachment*:The ND-UA-NHS was immersed in a solution of CPT dissolved in dry DMF at a concentration of 2.5 mg mL^{-1}. The ND-UA-NHS was incubated in the solution in the dark for 24 h, followed by centrifugation and evaporation of the DMF under vacuum. The ND-UA-NHS were then rinsed with ethanol and dried under vacuum (ethanol used for rinsing was kept for CPT concentration measurement). 2 mg mL^{-1} of the MLR2 antibody was suspended in 1X PBS buffer (pH 7.4). The pSi NDs were resuspended in the antibody solution. The reaction was carried out for 30 min, following which the pSi NDs were recovered using centrifugation and resuspended in 1X PBS (pH 7.4).

Fluorescent Antibody Attachment and Characterization: Dylight 549-conjugated mouse antihuman IgG antibodies (Abcam, Australia) were obtained at 1 mg mL^{-1} concentrations. 1 mL of antibody solution was oxidized according to subsection (b) under the "pSi NDs Functionalization with Semicarbazide" section. pSi NDs functionalized according to section "ND functionalization with undecylenic Acid" (deprotected semicarbazide) (not loaded with CPT) was incubated with the oxidized antibody, while nonoxidized antibodies were incubated with pSi NDs functionalized according to section "ND functionalization with undecylenic acid" (NHS/UA) and nonfunctionalized NDs. The incubation was performed for 16 h at 4 °C. The NDs were then rinsed with 1X PBS (pH 7.4) three times for 5 min each time to remove unattached antibodies. All the NDs were then examined using an inverted fluorescence microscope equipped with the appropriate filters (Nikon Eclipse Ti—S).

Determination of CPT Loading: CPT loading for each set of NDs was determined on the loading solution (before and after loading) as well as on the rinsing solutions using a HPLC system (Shimadzu Corporation, Japan) equipped with a series of LC-20ADXR pumps, SIL-20ACXR auto sampler, CTO-20AC column oven, SPD20A variable UV detector that was set up to measure at 380 nm, and a LiChrospher C18 analytical column (RP-18, 5 µm, 4.6 mm ID × 250 mm). The mobile phase consisted of a mixture of 10 mM phosphoric acid and acetonitrile at 1:1 v/v and pH = 3.0. The mobile phase was eluted with a flow rate of 1.2 mL min^{-1}. Using this set of conditions, the limit of detection was 8 ng mL^{-1} and the limit of quantification was 24 ng mL^{-1}. Linear calibration curves with $R^2 \geq 0.99$ were plotted for the peak areas obtained through chromatography versus drug concentrations over the range of 0.05–50 µg mL^{-1} without using an internal standard. All dilutions were prepared using the mobile phase to establish a final concentration range suitable for HPLC quantification.

Determination of CPT Release Kinetics: CPT release was measured using a Cary Eclipse fluorescence spectrometer (Agilent Technologies) fitted with a Peltier temperature control system in real time from pSi NDs prepared according to sections "pSi NDs functionalization with semicarbazide" and "ND functionalization with undecylenic acid". The NDs were suspended at a concentration of 33.3 µg mL^{-1} in 3 mL of cell culture media and added to standard quartz cuvettes. The cell culture media was preheated to 37 °C and the release experiment was carried out at the same temperature for 24 h while collecting fluorescence measurements every 5 min. The excitation wavelength was set to 340 nm and emission was detected at 440 nm.

ND Degradation Assay: A molybdenum blue colorimetric assay was employed to establish the released concentration of silicic acid from pSi NDs. Three sets of pSi NDs (nonfunctionalized NDs, ND-SC, and ND-UA) each weighing around 100 µg were each immersed in a buffer solution of tris(hydroxymethyl)aminomethane (Tris) (2 mL, pH = 7.2). Tris was used instead of PBS since phosphate in the PBS intereferes with the assay.[59] Measurements were taken by extracting 100 µL of solution every hour after a quick centrifugation step at 18 000 rpm to force the NDs to the bottom of the container. Each of the 100 µL aliquots were then added to 40 µL of 0.3 M HCl solution. This was followed by the addition of 20 µL of 42 mM ammonium molybdate. At this stage the solution was left to react for ≈10 min until the color changed to pale yellow. Next, 20 µL of the chelating agent ethylenediaminetetraacetic acid (27 mM) was added to the solution, following by 40 µL of 1.35 M sodium sulfite. After 1 h incubation at room temperature, the solution turned to a light blue color, the intensity of which was then measured using a kinetic microplate reader (VMax, Molecular Devices, USA) at 650 nm. Additionally, a standard set of silicic acid solutions was prepared to establish a calibration curve. For this purpose, sodium metasilicate

was used as the source of silicic acid and 11 dilutions were prepared in Tris buffer covering the range of 0–100 μM.

Infrared Spectroscopy: IR analysis was carried out on functionalized and nonfunctionalized pSi NDs. The NDs were deposited from solution onto a p-type 3–6 Ω cm flat Si wafer and allowed to dry. Analysis was performed on a Hyperion 1000 FTIR-Microscope coupled to a Vertex 70 IR source (Bruker, Germany) and a liquid N_2-cooled MCT detector. An attenuated total reflectance accessory with a germanium crystal was used directly onto the deposited NDs. The flat Si wafer was used as background. Spectra were acquired between 650 and 4000 cm^{-1} with a resolution of 4 cm^{-1} for 64 scans.

Cell Culture: SH-SY5Y and BSR cells were seeded in a 96 well plate at a concentration of 10^4 cells per well and left for 24 h. Subsequently, the cells were incubated with NDs prepared according to sections "pSi NDs Functionalization with Semicarbazide" and "ND functionalization with undecylenic acid". For the ND-SC, the following set of samples was used: nonfunctionalized NDs (ND), CPT-loaded NDs (ND-CPT), MLR2 antibody-functionalized NDs (ND-MLR2), and CPT-loaded and MLR2 antibody-functionalized NDs (ND-CPT-MLR2). A similar set of samples was also used for the pSi NDs with NHS chemistry. The cells were incubated with each set of the NDs for 30 min at a concentration of 50 μg mL^{-1} at 37 °C and 5% CO_2. After incubation, the cells were washed with PBS to remove any unattached NDs and then incubated in Dulbecco's modified Eagle's medium (DMEM) (10% FBS, 100 U mL^{-1} penicillin and 100 μg mL^{-1} streptomycin) in 5% CO_2 at 37 °C for 48 h.

Determination of Cell Targeting of pSi NDs: For the determination of targeted pSi ND binding to SH-SY5Y cells, MLR2 antibodies was labeled with FITC as follows. 200 μL of MLR2 antibody (3.6 mg mL^{-1}) was mixed with 20 μL of 1 M sodium bicarbonate (pH 9.0). 10 mg of FITC was dissolved in 1 mL DMSO (Sigma, Australia) and 50 μL of the FITC solution was added to the MLR2 solution. The mixture was stirred for 1 h in the dark at room temperature. Following the labeling reaction, MLR2 antibody was purified from the unattached FITC using gel filtration in a Sephadex G25 column using a buffer solution of 0.1 M Na_2HPO_4 + 0.15 M NaCl (pH 7.2). The fluorescent MLR2 antibody (FITC-MLR2) was attached to pSi NDs as described in sections "pSi NDs functionalization with semicarbazide" and "ND functionalization with undecylenic acid". The FITC-MLR2 antibody-functionalized NDs were then incubated with SH-SY5Y and BSR cells according to section "determination of cell targeting of pSi NDs", but the cells were grown on coverslips with a density of 5×10^4 cell cm^{-2} instead. In order to characterize the pSi ND attachment using fluorescence microscopy, the following steps were performed. ND-treated BSR and SH-SY5Y cells were fixed with a solution containing 4% paraformaldehyde (EM grade, Electron Microscopy Sciences) for 10 min, following which the cells were permeabilized with 0.1% Triton X-100 (Sigma-Aldrich) for 5 min at room temperature. The nuclei of the cells were stained with 1 μg mL^{-1} Hoechst 33342 (Life Technologies) for 15 min at room temperature. This was followed by staining the actin filaments in the cytoplasm with 100 μM TRITC-labeled phalloidin (Sigma-Aldrich) for 45 min. Finally, the coverslips were washed in PBS and mounted using fluorogel mounting reagent (ProSciTech). The cells were imaged using a confocal fluorescence microscope (Nikon A1, Japan) equipped with the appropriate filters and lasers. The ND uptake by cells was quantified from the blue (Hoechst 33342, nucleus) and green (ND fluorescence) channels of the fluorescence microscopy images. ImageJ software (NIH) was used to count the number of nuclei and NDs in each image. ND quantification was performed in triplicates for each cell type and linker chemistry, with a minimum cell population count of $n = 150$ cells. The values are stated as the number of NDs per cell nucleus.

In Vitro Cell Viability Assay: The viability of cells prepared according to section "determination of cell targeting of pSi NDs" was determined using a commercial LDH assay kit (LDH-Cytotoxicity Assay Kit II, Abcam) according to the manufacturer's instructions. 100 μL of the cell suspension was centrifuged at 600× g for 10 min and the supernatant was transferred into a 96 well plate. To each well, 100 μL of the LDH reaction mix was added. After 30 min of incubation at room temperature, the absorbance was measured at 450 nm using a NanoDrop 2000 UV/Vis spectrometer (Thermo Scientific, Australia). LDH measurements were performed in triplicate. The cytotoxicity of NDs was calculated by comparison of LDH secretion of test samples against untreated cell (reference 1) and fully lyzed cell (reference 2) references:

$$\text{Cytotoxicity \%} = \frac{\text{Test Sample} - \text{Ref 2}}{\text{Ref 1} - \text{Ref 2}} \times 100\%$$

The percentage viability (%) was calculated as follows:

$$\text{Viability \%} = 100\% - \text{Cytotoxicity \%}$$

Preparation of Cells for SEM: Cells prepared according to section "determination of cell targeting of pSi NDs" were treated with 1% osmium tetroxide for 30 min at room temperature, and then rinsed in PBS for 10 min three times. This was followed by gradual dehydration using successively increasing ethanol concentrations (50%, 70%, 90%, and 100%) with 15 min for each wash. The cells were then chemically dried using hexamethyldisilazane (HMDS) first with 1:1 ethanol:HMDS followed by 1:3 ethanol:HDMS, and finally 100% HDMS. The HDMS was drained and the cells were allowed to dry for 5 min, followed by sputter coating a layer of platinum (Pt) with 20 nm thickness.

Scanning Electron Microscopy: SEM imaging was carried out using a Quanta 450 FEG Environmental SEM (FEI, Netherlands) fitted with a solid state detector and operating at 30 kV in high vacuum mode. Measurements of particle dimensions were performed using the freely available software ImageJ.

Transmission Electron Microscopy: pSi NDs were characterized with a computer-controlled TEM JEM-2100F (Jeol Pty Ltd), equipped with a field emission gun. Samples were suspended in ethanol (≈100 μg mL^{-1}) to ensure the rapid evaporation of the solvent on a 300 lines/mesh copper grid coated with a Formvar film (PST ProSciTech). The high-resolution pole was operated at a 200 kV accelerating voltage and images were acquired with a Gatan Orius SC1000 CCD camera mounted at the bottom of the column. The pore size distribution was measured using the freely available software ImageJ.

Supporting Information

Supporting Information is available from the Wiley Online Library or from the author.

Acknowledgements

This work was performed (in part) at the South Australian node of the Australian National Fabrication Facility under the National Collaborative Research Infrastructure Strategy to provide nano- and microfabrication facilities for Australia's researchers. The authors would like to thank Marc Cirera for providing them with the schematic representation of the fabrication process shown in Scheme 1. They would also like to acknowledge Dr. Shasha Rao for her work conducting the HPLC concentration measurements. H.A. and B.D. have contributed equally to this work.

Received: September 30, 2014
Revised: November 6, 2014
Published online: December 15, 2014

[1] M. Gaumet, A. Vargas, R. Gurny, F. Delie, *Eur. J. Pharm. Biopharm.* **2008**, *69*, 1.
[2] K. Cho, X. Wang, S. Nie, Z. Chen, D. M. Shin, *Clin. Cancer Res.* **2008**, *14*, 1310.

[3] H. Maeda, *Adv. Enzyme Regul.* **2001**, *41*, 189.
[4] T. M. Allen, *Nat. Rev. Cancer* **2002**, *2*, 750.
[5] E. Secret, K. Smith, V. Dubljevic, E. Moore, P. Macardle, B. Delalat, M.-L. Rogers, T. G. Johns, J.-O. Durand, F. Cunin, N. H. Voelcker, *Adv. Healthcare Mater.* **2013**, *2*, 718.
[6] I. I. Slowing, J. L. Vivero-Escoto, C.-W. Wu, V. S. Y. Lin, *Adv. Drug Delivery Rev.* **2008**, *60*, 1278.
[7] B. Godin, C. Chiappini, S. Srinivasan, J. F. Alexander, K. Yokoi, M. Ferrari, P. Decuzzi, X. Liu, *Adv. Funct. Mater.* **2012**, *22*, 4225.
[8] I. Ahmad, M. Longenecker, J. Samuel, T. M. Allen, *Cancer Res.* **1993**, *53*, 1484.
[9] M. L. Krieger, N. Eckstein, V. Schneider, M. Koch, H.-D. Royer, U. Jaehde, G. Bendas, *Int. J. Pharm.* **2010**, *389*, 10.
[10] H. Pinto-Alphandary, A. Andremont, P. Couvreur, *Int. J. Antimicrob. Agents* **2000**, *13*, 155.
[11] M. L. Hans, A. M. Lowman, *Curr. Opin. Solid State Mater. Sci.* **2002**, *6*, 319.
[12] J. Panyam, V. Labhasetwar, *Adv. Drug Delivery Rev.* **2003**, *55*, 329.
[13] K. Yin Win, S.-S. Feng, *Biomaterials* **2005**, *26*, 2713.
[14] A. V. Ambade, E. N. Savariar, S. Thayumanavan, *Mol. Pharm.* **2005**, *2*, 264.
[15] N. Nasongkla, E. Bey, J. Ren, H. Ai, C. Khemtong, J. S. Guthi, S.-F. Chin, A. D. Sherry, D. A. Boothman, J. Gao, *Nano Lett.* **2006**, *6*, 2427.
[16] M. Gary-Bobo, Y. Mir, C. Rouxel, D. Brevet, O. Hocine, M. Maynadier, A. Gallud, A. Da Silva, O. Mongin, M. Blanchard-Desce, S. Richeter, B. Loock, P. Maillard, A. Morère, M. Garcia, L. Raehm, J.-O. Durand, *Int. J. Pharm.* **2012**, *432*, 99.
[17] S.-H. Wu, Y. Hung, C.-Y. Mou, *Chem. Commun.* **2011**, *47*, 9972.
[18] F. Peng, Y. Su, X. Wei, Y. Lu, Y. Zhou, Y. Zhong, S.-T. Lee, Y. He, *Angew. Chem Int. Ed.* **2013**, *52*, 1457.
[19] J.-H. Park, L. Gu, G. von Maltzahn, E. Ruoslahti, S. N. Bhatia, M. J. Sailor, *Nat. Mater.* **2009**, *8*, 331.
[20] J. F. Popplewell, S. J. King, J. P. Day, P. Ackrill, L. K. Fifield, R. G. Cresswell, M. L. di Tada, K. Liu, *J. Inorg. Biochem.* **1998**, *69*, 177.
[21] M. Vallet-Regí, F. Balas, D. Arcos, *Angew. Chem Int. Ed.* **2007**, *46*, 7548.
[22] R. A. Bley, S. M. Kauzlarich, J. E. Davis, H. W. H. Lee, *Chem. Mater.* **1996**, *8*, 1881.
[23] J. Salonen, L. Laitinen, A. M. Kaukonen, J. Tuura, M. Björkqvist, T. Heikkilä, K. Vähä-Heikkilä, J. Hirvonen, V. P. Lehto, *J. Controlled Release* **2005**, *108*, 362.
[24] F. Lu, S.-H. Wu, Y. Hung, C.-Y. Mou, *Small* **2009**, *5*, 1408.
[25] Y.-S. Lin, C. L. Haynes, *J. Am. Chem. Soc.* **2010**, *132*, 4834.
[26] J. A. Champion, S. Mitragotri, *Proc. Natl. Acad. Sci. U.S.A.* **2006**, *103*, 4930.
[27] J. A. Champion, Y. K. Katare, S. Mitragotri, *Proc. Natl. Acad. Sci. U.S.A.* **2007**, *104*, 11901.
[28] J. A. Champion, Y. K. Katare, S. Mitragotri, *J. Controlled Release* **2007**, *121*, 3.
[29] T.-R. Lee, M. Choi, A. M. Kopacz, S.-H. Yun, W. K. Liu, P. Decuzzi, *Sci. Rep.* **2013**, *3*.
[30] S. E. A. Gratton, P. A. Ropp, P. D. Pohlhaus, J. C. Luft, V. J. Madden, M. E. Napier, J. M. DeSimone, *Proc. Natl. Acad. Sci. U.S.A.* **2008**, *105*, 11613.
[31] P. Decuzzi, B. Godin, T. Tanaka, S. Y. Lee, C. Chiappini, X. Liu, M. Ferrari, *J. Controlled Release* **2010**, *141*, 320.
[32] P. Kolhar, A. C. Anselmo, V. Gupta, K. Pant, B. Prabhakarpandian, E. Ruoslahti, S. Mitragotri, *Proc. Natl. Acad. Sci. U.S.A.* **2013**, *110*, 10753.
[33] R. Toy, P. M. Peiris, K. B. Ghaghada, E. Karathanasis, *Nanomedicine* **2013**, *9*, 121.
[34] E. Tasciotti, X. Liu, R. Bhavane, K. Plant, A. D. Leonard, B. K. Price, M. M.-C. Cheng, P. Decuzzi, J. M. Tour, F. Robertson, M. Ferrari, *Nat. Nanotechnol.* **2008**, *3*, 151.
[35] A. I. Hochbaum, D. Gargas, Y. J. Hwang, P. Yang, *Nano Lett.* **2009**, *9*, 3550.
[36] L. Lin, S. Guo, X. Sun, J. Feng, Y. Wang, *Nanoscale Res. Lett.* **2010**, *5*, 1822.
[37] G. Yuan, R. Mitdank, A. Mogilatenko, S. F. Fischer, *J. Phys. Chem. C* **2012**, *116*, 13767.
[38] S. Weidemann, M. Kockert, D. Wallacher, M. Ramsteiner, A. Mogilatenko, K. Rademann, S. F. Fischer, arXiv preprint arXiv:1410.3763, **2014**.
[39] C. Chiappini, X. Liu, J. R. Fakhoury, M. Ferrari, *Adv. Funct. Mater.* **2010**, *20*, 2231.
[40] M. H. Kim, S. H. Im, O. O. Park, *Adv. Funct. Mater.* **2005**, *15*, 1329.
[41] K. Wostyn, Y. Zhao, B. Yee, K. Clays, A. Persoons, G. de Schaetzen, L. Hellemans, *J. Chem. Phys.* **2003**, *118*, 10752.
[42] V. J. Logeeswaran, N. P. Kobayashi, M. S. Islam, W. Wu, P. Chaturvedi, N. X. Fang, S. Y. Wang, R. S. Williams, *Nano Lett.* **2008**, *9*, 178.
[43] L. M. Bimbo, M. Sarparanta, H. A. Santos, A. J. Airaksinen, E. Mäkilä, T. Laaksonen, L. Peltonen, V.-P. Lehto, J. Hirvonen, J. Salonen, *ACS Nano* **2010**, *4*, 3023.
[44] P. G. Kuzmin, G. A. Shafeev, V. V. Bukin, S. V. Garnov, C. Farcau, R. Carles, B. N. D. Warot-Fontrose, V. R. Guieu, G. Viau, *J. Phys. Chem. C* **2010**, *114*, 15266.
[45] Y. Coffinier, C. Olivier, A. Perzyna, B. Grandidier, X. Wallart, J. O. Durand, O. Melnyk, D. Stiévenard, *Langmuir* **2005**, *21*, 1489.
[46] A. J. Simons, T. I. Cox, A. Loni, L. T. Canham, R. Blacker, *Thin Solid Films* **1997**, *297*, 281.
[47] L. H. Li, T. J. Fraser, E. J. Olin, B. K. Bhuyan, *Cancer Res.* **1972**, *32*, 2643.
[48] Q. Yin, R. Tong, L. Yin, T. M. Fan, J. Cheng, *Polym. Chem.* **2014**, *5*, 1581.
[49] J. Gottleib, A. Guarino, J. Call, *Cancer Chemother. Rep.* **1970**, *54*, 461.
[50] J. Williams, R. Lansdown, R. Sweitzer, M. Romanowski, R. LaBell, R. Ramaswami, E. Unger, *J. Controlled Release* **2003**, *91*, 167.
[51] J. Lu, M. Liong, J. I. Zink, F. Tamanoi, *Small* **2007**, *3*, 1341.
[52] P. Kinnari, E. Mäkilä, T. Heikkilä, J. Salonen, J. Hirvonen, H. A. Santos, *Int. J. Pharm.* **2011**, *414*, 148.
[53] A. Cifuentes-Rius, H. de Puig, J. C. Y. Kah, S. Borros, K. Hamad-Schifferli, *ACS Nano* **2013**, *7*, 10066.
[54] S. Wang, *Microporous Mesoporous Mater.* **2009**, *117*, 1.
[55] D. Matusica, M. P. Fenech, M.-L. Rogers, R. A. Rush, *J. Neurosci. Res.* **2008**, *86*, 553.
[56] C. Zhang, S. Helmsing, M. Zagrebelsky, T. Schirrmann, A. L. J. Marschall, M. Schüngel, M. Korte, M. Hust, S. Dübel, *PLoS One* **2012**, *7*, e30684.
[57] M.-L. Rogers, K. S. Smith, D. Matusica, M. Fenech, L. Hoffman, R. A. Rush, N. H. Voelcker, *Front. Mol. Neurosci.* **2014**, *7*, 80.
[58] M.-L. Rogers, I. Atmosukarto, D. A. Berhanu, D. Matusica, P. Macardle, R. A. Rush, *J. Neurosci. Methods* **2006**, *158*, 109.
[59] K. Yoshimura, M. Motomura, T. Tarutani, T. Shimono, *Anal. Chem.* **1984**, *56*, 2342.